AFRL-RX-TY-TP-2012-0041

MAGNETIC ROTATIONAL SPECTROSCOPY WITH NANORODS TO PROBE TIME-DEPENDENT RHEOLOGY OF MICRODROPLETS (POSTPRINT)

Alexander Tokarev, Igor Luzinov, and Konstantin G. Kornev
School of Materials Science and Engineering
161 Sirrine Hall
Clemson University
Clemson, SC 29634

Jeffery R. Owens
Airbase Technologies Division
Air Force Research Laboratory
139 Barnes Drive, Suite 2
Tyndall Air Force Base, FL 32403-5323

Contract No. FA8650-09-D-5900-0002

May 2012

AIR FORCE RESEARCH LABORATORY
MATERIALS AND MANUFACTURING DIRECTORATE

■ **Air Force Materiel Command** ■ **United States Air Force** ■ **Tyndall Air Force Base, FL 32403-5323**

REPORT DOCUMENTATION PAGE

Form Approved
OMB No. 0704-0188

PLEASE DO NOT RETURN YOUR FORM TO THE ABOVE ADDRESS.

1. REPORT DATE *(DD-MM-YYYY)*	2. REPORT TYPE	3. DATES COVERED *(From - To)*
10-MAY-2012	Journal Article - POSTPRINT	13-APR-2011 -- 18-JAN-2012

4. TITLE AND SUBTITLE

Magnetic Rotational Spectroscopy with Nanorods to Probe Time-Dependent Rheology of Microdroplets (POSTPRINT)

5a. CONTRACT NUMBER

FA8650-09-D-5900-0002

5b. GRANT NUMBER

5c. PROGRAM ELEMENT NUMBER

6. AUTHOR(S)

*Tokarev, Alexander; *Luzinov, Igor; #Owens, Jeffery R.; *Kornev, Konstantin G.

5d. PROJECT NUMBER

5e. TASK NUMBER

5f. WORK UNIT NUMBER

QL102011

7. PERFORMING ORGANIZATION NAME(S) AND ADDRESS(ES)

* School of Materials Science and Engineering
161 Sirrine Hall
Clemson University
Clemson, SC 29634

8. PERFORMING ORGANIZATION REPORT NUMBER

9. SPONSORING/MONITORING AGENCY NAME(S) AND ADDRESS(ES)

#Air Force Research Laboratory
Materials and Manufacturing Directorate
Airbase Technologies Division
139 Barnes Drive, Suite 2
Tyndall Air Force Base, FL 32403-5323

10. SPONSOR/MONITOR'S ACRONYM(S)

AFRL/RXQL

11. SPONSOR/MONITOR'S REPORT NUMBER(S)

AFRL-RX-TY-TP-2011-0041

12. DISTRIBUTION/AVAILABILITY STATEMENT

Distribution Statement A: Approved for public release; distribution unlimited.
Available only to DTIC users. U.S. Government or Federal Purpose Rights License.

13. SUPPLEMENTARY NOTES

Distribution Code 20: JOURNAL ARTICLES; DTIC USERS ONLY. Document contains color images. Ref Public Affairs Case # 88ABW-2012-3844, 11 July 2012. Published in Langmuir, 2012, 28 (26), pp 10064–10071 DOI: 10.1021/la3019474

14. ABSTRACT

Characterization of polymers during polymerization is a challenge. Especially difficult is to study kinetics of gel formation inside tiny droplets. In many cases, viscosity of these fluids increases exponentially fast. In this paper, the rheological properties of fluids were evaluated by examining the behavior of magnetic nanorods in rotating magnetic field. We proposed a theory describing the rotation of a magnetic nanorod in a fluid when its viscosity increases with time exponentially fast. To confirm the theory, we studied the rheology of poly(2-hydroxyethyl-methacrylate) (HEMA)-based hydrogel undergoing photopolymerization and cross-linking with diethylene dlycol dimethacylate (DEGDMA). We showed that magnetic rotational spectroscopy provides rich physico-chemical information about the gelation process. . . . . Remarkably, one can analyze not only the liquid state of the polymer, but the gel as well. Since the probing nanorods are measured in nanometers, this method can be used for the in vivo mapping of the rheological properties of biofluids and polymers on a microscopic level at short time intervals when other methods fail short.

15. SUBJECT TERMS

rheology, nanorods, viscosity, EM, electromagnetic

16. SECURITY CLASSIFICATION OF:			17. LIMITATION OF ABSTRACT	18. NUMBER OF PAGES	19a. NAME OF RESPONSIBLE PERSON
a. REPORT	b. ABSTRACT	c. THIS PAGE			Jeffery R. Owens
U	U	U	UU	10	19b. TELEPHONE NUMBER *(Include area code)*

Reset

Standard Form 298 (Rev. 8/98)
Prescribed by ANSI Std. Z39.18

Langmuir

Article

pubs.acs.org/Langmuir

Magnetic Rotational Spectroscopy with Nanorods to Probe Time-Dependent Rheology of Microdroplets

Alexander Tokarev,[†] Igor Luzinov,[†] Jeffery R. Owens,[‡] and Konstantin G. Kornev*,[†]

[†]School of Materials Science and Engineering, 161 Sirrine Hall, Clemson University, Clemson, South Carolina 29634, United States

[‡]Air Force Research Laboratory, Airbase Technology Division, Airbase Scientific Branch, Tyndall AFB, Panama City, Florida 32403, United States

Supporting Information

ABSTRACT: In situ characterization of minute amounts of fluids that rapidly change their rheological properties is a challenge. In this paper, the rheological properties of fluids were evaluated by examining the behavior of magnetic nanorods in a rotating magnetic field. We proposed a theory describing the rotation of a magnetic nanorod in a fluid when its viscosity increases with time exponentially fast. To confirm the theory, we studied the time-dependent rheology of microdroplets of 2-hydroxyethyl-methacrylate (HEMA)/diethylene glycol dimethacylate (DEGDMA)-based hydrogel during photopolymerization synthesis. We demonstrated that magnetic rotational spectroscopy provides rich physicochemical information about the gelation process. The method allows one to completely specify the time-dependent viscosity by directly measuring characteristic viscosity and characteristic time. Remarkably, one can analyze not only the polymer solution, but also the suspension enriched with the gel domains being formed. Since the probing nanorods are measured in nanometers, this method can be used for the in vivo mapping of the rheological properties of biofluids and polymers on a microscopic level at short time intervals when other methods fall short.

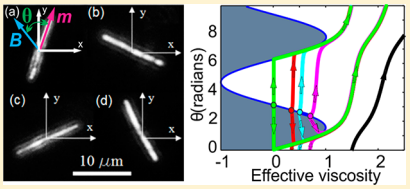

1. INTRODUCTION

Many polymers and biofluids rapidly react on the environmental conditions by changing their rheological properties.[1] Rheology of polymer solutions/gels (e.g., hazardous fluids containing thickeners) and biofluids depends on the concentration, level of cross-linking, oxygen content, temperature, pH, and many other environmental parameters. In biofluids such as cellular, mucosal, and tissue fluids, the fluid viscosity changes over time making it challenging to quantify and analyze these changes. Drastic thickening of fluids over a short time interval often results in far-reaching consequences; for example, sickle cell disease results in the increase of cytosolic viscosity inside the red blood cells,[2,3] and polymerization of fibrinogen leads to fibrin clot formation and wound healing.[4−6] In polymer/biomedical engineering, fast polymerization processes are frequently used for different applications; for example, by HEMA (2-hydroxyethyl-methacrylate) photopolymerization one can make contact disposable lenses.[7−10] Alginate and other polysaccharides, gelling in fractions of a second, are used for manufacturing fibers and films.[11] These broad applications and abundance of rapidly gelling systems call for methods of their analyses and characterization. The physics of nucleation and the associated rheological fingerprints of the gelation process are hidden at the nanoscale and almost indistinguishable at the microscale. The available rheological techniques fall short of providing viable information about the in vivo physicochemical reactions and gelation mechanisms in the real time[1] especially when the amount of liquids is limited to microdroplets.[3,12]

A number of the microrheological methods were recently developed to study the rheology inside the living cells.[13−15] These methods are summarized in ref 16. Typically, a probe in the form of a solid particle is embedded into the cell and one measures its response to the thermal fluctuations (passive microrheology[15]) or to the external field, for example, magnetic field (active microrheology[14]). Active microrheology was used to study the rheological properties of different fluids.[17−19] Magnetic rotational spectroscopy (MRS) is a part of active microrheology where magnetic nanorods with unique rotational features deserve a special attention.[20−26] In the past decade, the most attention has been paid to the development of MRS for simple Newtonian fluids. In this Article, we develop an MRS which can be used to study the rheological properties of non-Newtonian fluids with an exponentially fast-growing viscosity. We believe that the MRS described here will provide biophysicists and chemists with a unique tool to probe and map the physicochemical properties of sophisticated microsystems in short time intervals.

As an illustration of the robustness of the proposed method, we use UV polymerization of HEMA to analyze its time-dependent viscosity. The HEMA viscosity exponentially increases during free radical (three-dimensional UV) polymerization in the presence of the cross-linker DEGDMA (diethylene glycol dimethacylate).[7] The gel point for the system can be reached in 60−200 s depending on the DEGDMA concentration.[7] HEMA polymerizes linearly

Received: March 13, 2012

   dx.doi.org/10.1021/la3019474 | *Langmuir* XXXX, XXX, XXX−XXX

through the carbon−carbon double bond and cross-links through the two carbon−carbon double bonds present in DEGDMA (see Supporting Information and Figure S1 for details).

The time-dependent viscosity of many monomers undergoing polymerization is typically described by the following equation:[7,9]

$$\eta(t) = \eta_0 \, e^{t/\tau} \tag{1}$$

where η_0 is the initial viscosity of monomer solution, t is the time, and τ is the characteristic time of polymerization. This characteristic time is considered a phenomenological parameter of the polymerization process.[7,9] The physics of exponential thickening of fluid via three-dimensional polymerization is not completely understood, yet some key mechanisms leading to this effect have been identified.[10]

In order to assess the polymerization kinetics using rheological data, it is therefore imperative to correlate the kinetic parameters with the rheological parameters η_0 and τ. The existing basic MRS model does not take into account the time dependence of the fluid viscosity. We therefore develop a model to describe the dynamics of rotation of a magnetic nanorod in a fluid with an exponentially increasing viscosity. Then, we apply this model to study the gelation kinetics of HEMA during photopolymerization. We analyze the experimental data on rotation of magnetic nanorods and perform the FT-IR measurements of the HEMA solutions during photopolymerization. All these experiments show the robustness of the proposed MRS method allowing us to find a relation between the phenomenological parameters η_0 and τ, concentration of the cross-linker, and the fraction of the cross-linked material at different stages of photopolymerization.

2. THEORY

2.1. Model. The movement of a magnetic nanorod in a rotating magnetic field is shown in Figure 1 (see movie S6 in Supporting Information). The angle α specifies the direction of applied magnetic field **B** with respect to the reference axis X. Since the applied field rotates at a constant rate, this angle depends linearly on time, $\alpha = 2\pi ft$, where f is the frequency of the rotating magnetic field. We assume that the magnetization vector **M** is directed parallel to the nanorod axis. The drag force resists the nanorod rotation causing the nanorod to lag behind the field, making angle θ with vector **B** (Figure 1). In order to derive an equation governing the nanorod rotation, it is convenient to count its revolutions with respect to the fixed system of coordinates, i.e., with respect to the X-axis. Therefore, if the nanorod axis makes the angle $\varphi(t)$ with the X-axis, this angle can be connected with $\alpha(t)$ and $\theta(t)$ as $\varphi(t) = 2\pi ft - \theta(t)$.

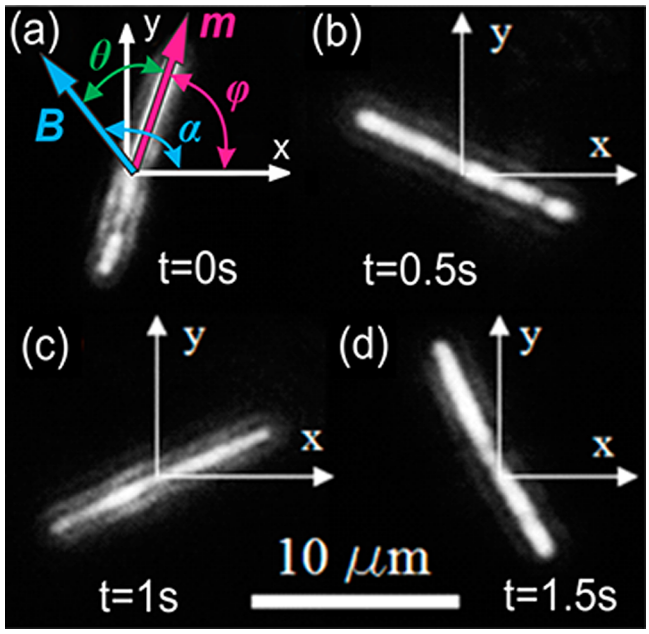

Figure 1. Counter clockwise rotation of nickel nanorod (d = 200 nm in diameter) in a plane. Uniform magnetic field rotates with constant frequency f = 0.5 Hz forcing the nanorod to follow it.

The torque balance equation reads $(\gamma d\varphi/dt)\mathbf{e} = \mathbf{M} \times \mathbf{B}$, where γ is the drag coefficient, and **e** is the unit vector directed perpendicularly to the plane of the nanorod rotation.[27,28] Substituting the definition of angle $\varphi(t)$ through the angles $\alpha(t)$ and $\theta(t)$, the governing equation takes on the following form:[22,24]

$$\gamma\left(2\pi f - \frac{d\theta}{dt}\right) = mB \sin\theta \tag{2}$$

where m is the magnetic moment of the nanorod. The drag coefficient depends on the nanorod length l, its diameter d, and liquid viscosity $\eta(t) = \eta_0 \exp(t/\tau)$ as

$$\gamma(t) = \frac{\eta_0 \, e^{t/\tau} l^3 \pi}{3\ln(l/d) - A} \tag{3}$$

where constant $A \approx 2.4$ was calculated in ref 29.

In the case of a constant viscosity, $\tau \to \infty$, eq 2 has a particular solution $2\pi f\gamma = mB \sin\theta$. This solution implies that the nanorod follows the rotating magnetic field **B** making angle θ with the field. When the frequency increases above the critical frequency

$$f_{cr} = mB \sin\theta / 2\pi\gamma \tag{4}$$

the nanorod slows down its rotation.[20,22] This critical frequency is easy to observe experimentally.[18,20,30] Obtaining this parameter from experiments, one can infer the viscosity of the surrounding fluid by solving eq 4 for γ and then applying eq 3 as $\tau \to \infty$ and solving it for η_0.

When the viscosity is not constant, we cannot use eq 4 anymore. Hence, the analysis of eq 2 deserves special care. We analyze this case by introducing the dimensionless times $T = 2\pi ft$ and $T_0 = 2\pi f\tau$. Then, eq 2 can be rewritten as $\beta \, e^{T/T_0}(1 - d\theta/dT) = \sin(\theta)$, where

$$\beta = \frac{\eta_0 l^3 2\pi f}{mB[3\ln(l/d) - A]} \tag{5}$$

After making this nondimensionalization, all physical parameters of our problem collapse into two dimensionless complexes, β and T_0. The dimensionless parameter β describes all possible scenarios of the nanorod rotation: assume first that the drag force is much greater than the magnetic torque. This implies that the dimensionless parameter β is much greater than 1, $\beta \gg 1$. Hence, as follows from the governing equation, $(1 - d\theta/dT) = (1/\beta)e^{-T/T_0} \sin(\theta) \approx 0$, or $\theta \approx T$, i.e., one would not expect any rotation of the magnetic nanorod. In the other limit, when the drag force is much smaller than the magnetic torque, the β-parameter is much smaller than 1, $\beta \ll$

dx.doi.org/10.1021/la3019474 | Langmuir XXXX, XXX, XXX−XXX

1. As follows from the governing equation, $\beta\, e^{T/T_0}(1 - d\theta/dT) = \sin(\theta)$, one would expect to observe the nanorod rotation until the left-hand side is smaller than 1.

For complete analysis of the nanorod rotation, it is convenient to introduce new auxiliary function $U = \beta e^{T/T_0}$. Then, eq 2 is rewritten as a system of two first-order differential equations

$$d\theta/dT = 1 - \sin\theta/U$$
$$dU/dT = U/T_0 \quad (6)$$

Dividing the first equation into the second, we obtain

$$\frac{d\theta}{dU} = \frac{T_0}{U^2}(U - \sin\theta) \quad (7)$$

Equation 7 allows one to perform a complete analysis of the nanorod dynamics depending on the viscosity, nanorod magnetization, magnetic field, and initial conditions. According to the definition of function U, the initial condition for this function reads $U(0) = \beta$. Therefore, in the plane (U, θ), each vertical line $U(0) = \beta$ corresponds to a continuous set of initial angles $\theta(0) = \theta_0$. Equation 7 has many solutions, but the nanorod dynamics is described by a single solution corresponding to finite interval.

2.2. Numerical Analysis. *Dynamics of Nanorods Starting Rotation at $\varphi(0) = 0$.* For an interpretation of the images of rotating nanorods, we need to follow the $\varphi(t)$-dependence. Therefore, we rewrite the torque balance equation in the following form $\gamma(t)\, d\varphi/dt = mB \sin(2\pi ft - \varphi)$. As an initial condition, we can always choose $\varphi(0) = 0$ implying that the nanorod is initially aligned with the field. The right-hand side of this equation is positive within the time interval $t < t_c$, where t_c is the first root of the equation $2\pi ft_c - \varphi(t_c) = 0$. This root is well-defined for each τ: it corresponds to the first maximum of function $\varphi(t)$. In Figure 2a, we show the behavior of the nanorod with length $l = 5$ μm, diameter $d = 0.2$ μm, initial viscosity of the HEMA solution $\eta_0 = 2.7$ mPa·s, magnetic field $B = 0.0015$ T, and frequency of the rotating field $f = 0.5$ Hz.

In Figure 2a, the nanorod revolves seven times at the frequency of the rotating field, and the dashed and solid lines corresponding to the field and nanorod rotation angles, respectively, coincide. On the other hand, the dash−dot line corresponding to the θ-angle remains at zero. Thus, during this rotation period, the field and magnetization are oriented parallel to each other. After seven turns, the slope of the red line changes, implying a gradual decrease of the rotation rate from 0.5 to 0.45 Hz. It can be seen from the graphs that the nanorod (φ) follows the rotation of the field (α) for about $N_{cr} = 11.17 \approx 11$ revolutions. After N_{cr} turns, the derivative of $\varphi(N)$ changes sign from positive to negative and the nanorod sways back for about 45° (see movie S7 in Supporting Information). After that, the nanorod rotates back and forth with decreasing amplitude and then completely stops at $N \approx 15$. In experiments, N_{cr} can be found by measuring the time (or number of turns) that the nanorod takes on before it sways back for the first time. In Figure 2b, we plot the dependence of this critical parameter N_{cr} as a function of T_0 and β.

One can infer from these dependencies that the number of turns significantly decreases as the initial viscosity increases and as the external field increases. This analysis suggests an experimental strategy for the investigation of rheological properties of polymeric fluids during polymerization. That is,

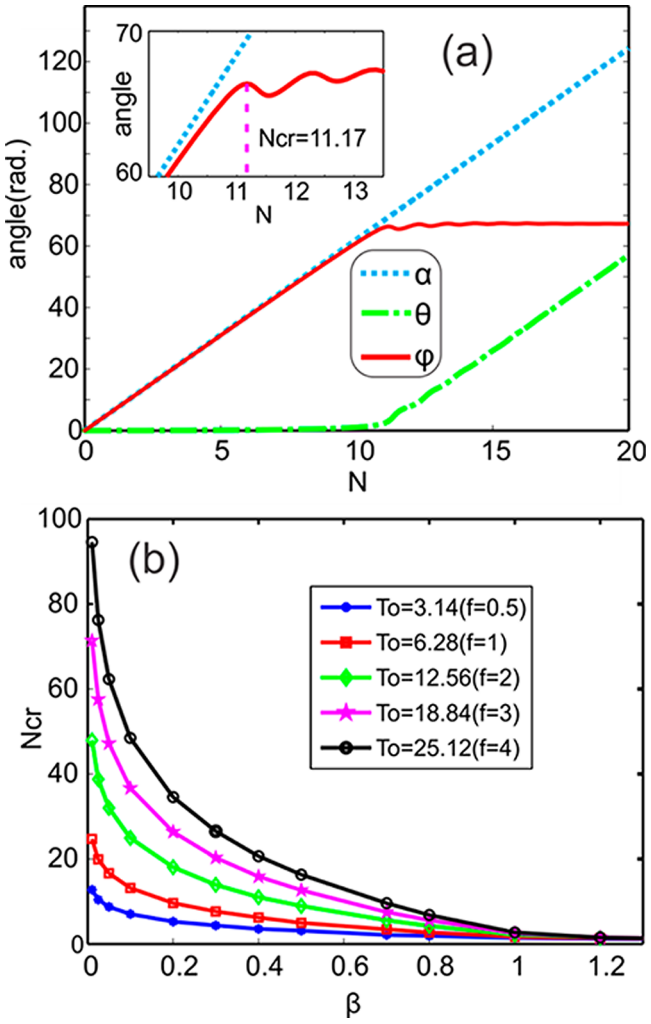

Figure 2. (a) Numerical solutions for φ, α, and θ as functions of the number of turns, $N = tf$, of a nanorod. The inset shows oscillating behavior of a nanorod which is about to stop its rotation after $N_{cr} \sim 11$ revolutions. (b) Dependence of the critical number of turns of a nanorod on parameter β.

one needs to measure N_{cr} and use τ as an adjustable parameter to fit the experimental N_{cr} with the theoretical one.

Dynamics of Nanorods Starting Rotation at Arbitrary Angle θ_0. There are three possible scenarios of nanorod rotation starting at an arbitrary angle θ_0. The results of numerical analysis of eq 7 are summarized in the form of the phase portrait shown in Figure 3. The initial conditions satisfying the inequality $U_0 = \beta < 1$ correspond to the case when the magnetic torque is stronger than that caused by the viscous drag. The shaded region under curve $U = \sin\theta$ corresponds to the conditions that cause the rod to sway toward the field direction at the initial instance of time. When the viscous drag takes over, the rod slows down its rotation and eventually stops. Since magnetic field keeps revolving, the angle $\theta(U)$ increases with each revolution even if the nanorod is not moving. Therefore, the integral curves coming out from the shaded region first decrease, form minimums at curve $U = \sin\theta$, and then turn up to increase.

This behavior can be easily observed by first aligning the nanorods with a bias field and then applying the rotating field which is directed perpendicular to the nanorods at $t = 0$. Therefore, the initial condition for this experiment is stated as

dx.doi.org/10.1021/la3019474 | Langmuir XXXX, XXX, XXX−XXX

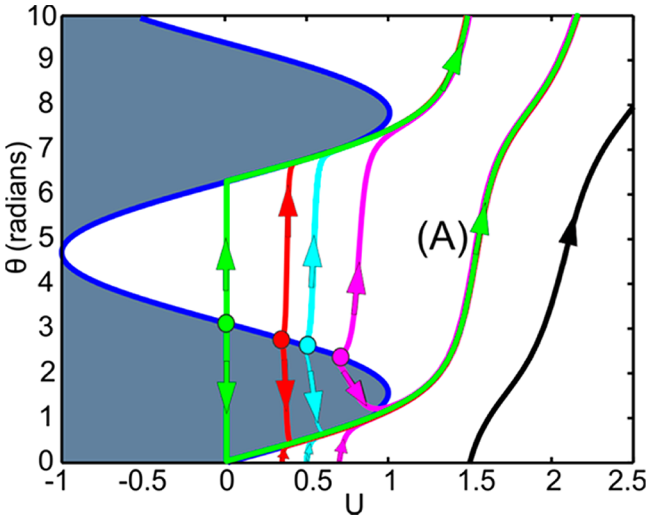

Figure 3. Phase portrait for eq 6 showing the solution behavior for different initial conditions U_0 and θ_0 at fixed dimensionless $T_0 = \pi$. Only $U > 0$ is of practical interest; hence, the integral curves for $U < 0$ are not shown.

$\theta_0 = \pi/2$. The time when the nanorods form the minimum angle θ_{min} with the rotating field can be thus obtained as $\beta e^{T_{min}/T_0} = \sin\theta_{min}$ or $T_{min} = 2\pi f\tau \ln(\sin\theta_{min}/\beta)$. Since θ_{min} and T_{min} are well-defined experimentally, one can infer the τ parameter from this relation.

Numerical analysis shows that all curves coming out of the shaded region first pass a minimum, then find their way to move at a close proximity of curve (A). When U is large, $U \gg 1$, eq 7 can be integrated to give $\theta = T_0 \ln U$, which means that angle θ increases linearly with time. These asymptotes explains why all integral curves run parallel to each other as U increases.

The integral curves coming out from the regions outside the shaded area in Figure 3, always increase as U increases. Therefore, as follows from the definition of angle θ, we have the following inequality $d\theta/dt = 2\pi f - d\varphi/dt > 0$. Rewriting this inequality for the observable angle, we obtain $2\pi f > d\varphi/dt$. This behavior suggests that the external field rotates faster than the rod for these initial conditions. The phase portrait sketched in Figure 3 is applicable for all T_0, yet the slopes of the integral curves are influenced by this parameter T_0.

The characteristic features of the nanorod behavior can be further elucidated by following the trajectories belonging to different regions on the phase portrait. For example, the initial conditions $\theta_0 = 0$, 2, and 2.9 correspond to three different types of the nanorod trajectories. From equation $\varphi(t) = \alpha(t) - \theta(t)$, one can infer the following initial condition for φ-solutions: $\varphi(0) = -\theta(0)$. The results of these calculations are presented in Figure 4 for physical parameter $\tau = 4$.

Figure 4a shows three different dependencies of angle θ on parameter U at different initial conditions θ_0, and the same $U(0) = 0.5$. In region $U > \sin(\theta_0)$, the initial viscous drag is stronger than the magnetic torque; hence, the field revolves faster than the nanorod. As follows from eq 7, the derivative $d\theta/dU$ is positive. With time, the viscous drag increases exponentially; hence, the field keeps revolving faster than the nanorod rotates. For initial condition $\theta_0 = 0$, the magnetic field and nanorod magnetization are initially coaligned (Figure 4a,b,c). As shown in Figure 4b, after approximately 0.2 revolutions, the angle θ stops changing. This implies that the nanorods are caught by the field for some time (Figure 4c). Then, after rotation in unison with the field for approximately 2 revolutions, the frequency of nanorod rotation starts to slow down. The nanorod sways back for the first time at $N_{cr} \cong 4$.

The dash−dot trajectory corresponding to the initial condition $\theta_0 = 2$ in Figure 4 a,b,c shows the distinct features of the trajectories with initial conditions taken from region $U < \sin(\theta_0)$. In this region, the magnetic torque is stronger than the viscous drag. Rotating magnetic field attempts to turn the nanorod toward the field direction. Simultaneously, the field keeps rotating toward the nanorod. This results in a decrease of the angle θ as dictated by eq 7 showing negative derivative $d\theta/dU$ in the region in question. After approximately 0.2 revolutions, the angle θ stops changing (Figure 4b). This means that the nanorods are caught by the field for some time repeating the behavior of nanorods which started at $\theta_0 = 0$ (the dash−dot line in Figure 4c). Then, after rotation in unison with the field for approximately 2 revolutions, the frequency of nanorod rotation starts to slow down. The nanorod sways back for the first time at $N_{cr} \cong 4$.

The dotted trajectory corresponding to the initial condition $\theta_0 = 2.9$ in Figure 4 a,b,c elucidates the distinct features of the trajectories with the initial conditions taken from region $U > \sin(\theta_0)$. In this region, the drag force is greater than the magnetic torque. The explanation of the nanorod behavior is analogous to that discussed above for $U > \sin(\theta_0)$, $\theta_0 = 0$.

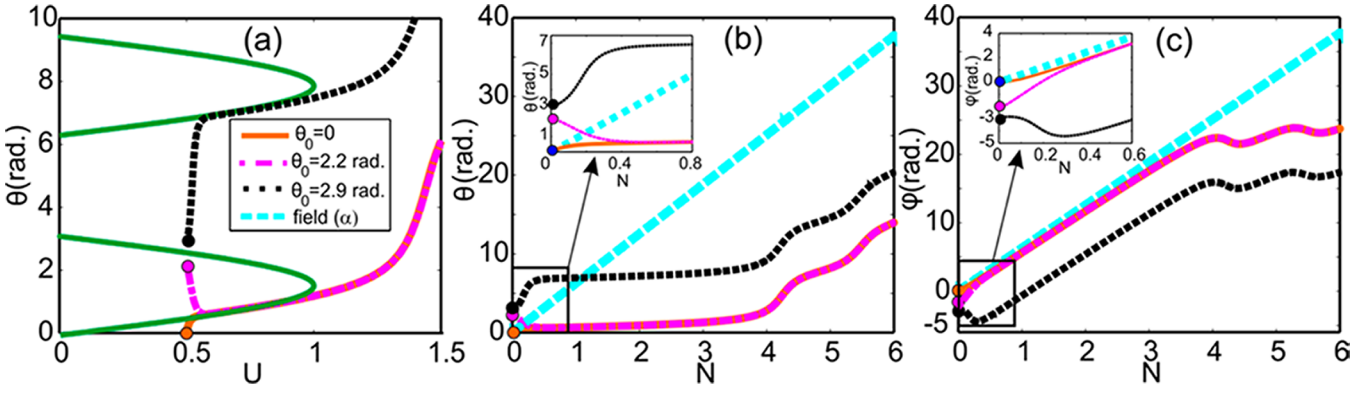

Figure 4. Nanorod behavior at three initial conditions, $\theta_0 = 0$, 2, and 2.9 radians. (a) Phase portrait of eq 7 showing the solution behavior for these initial conditions. (b) Numerical θ-solutions as a function of the number of turns, $N = t \cdot f$. (c) Numerical φ-solutions as a function of the number of turns.

dx.doi.org/10.1021/la3019474 | *Langmuir* XXXX, XXX, XXX−XXX

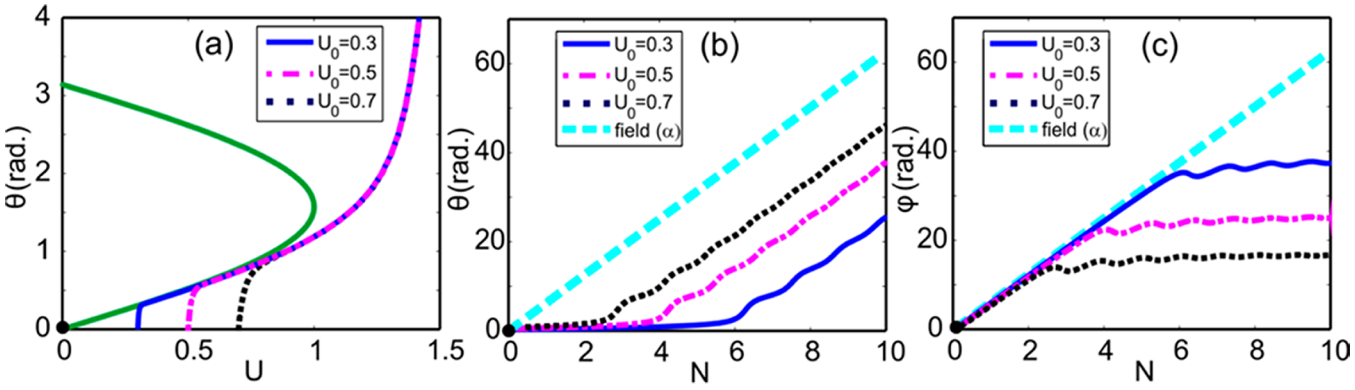

Figure 5. Nanorod behavior at different initial conditions $\beta = U(0) = 0.3, 0.5, 0.7$. (a) Phase portrait of eq 7 showing the solution behavior for different initial conditions $U(0)$ at $\theta_0 = 0$. (b) Numerical θ-solutions as a function of the number of turns, $N = t{\cdot}f$. (c) Numerical φ-solutions as a function of the number of turns.

For all these three cases, the parameter N_{cr} is the same, and it is equal to $N_{cr} \cong 4$. From the numerical analysis, we conclude that the behavior of nanorods at the first moments of time does depend on angle θ_0, but the critical number of turns N_{cr} does not depend on the initial orientation of the nanorods.

Effect of β-Parameter on Nanorod Dynamics. Effect of the β-parameter, i.e., the initial condition $U(0)$, can be explained by following the trajectories corresponding to $\beta = U_0 = 0.3$, 0.5, and 0.7 and assuming that the initial angle $\theta_0 = 0$. The dependencies of functions θ and φ on time are presented in Figure 5 where we have chosen $\tau = 4$.

Figure 5 reveals that the nanorod behavior for different β does not change significantly: the behavior of the θ-solutions on the number of turns is very similar among the solutions. The same is valid for the φ-solutions. At initial moments of time, the φ- and α-solutions coincide, i.e., the nanorods are coaligned with the field and revolve with the same frequency as that of the driving magnetic field (Figure 5c). The nanorod keeps rotating until it reaches a critical number of turns, N_{cr} . This critical number depends on the initial conditions; for example, $N_{cr}(0.3) = 2.8$, $N_{cr}(0.5) = 4$, $N_{cr}(0.7) = 6.1$. The lower the β-parameter, the greater the critical number of turns. As follows from eq 5, the β-parameter can be decreased by decreasing initial viscosity, or by making the nanorod shorter, or by applying a stronger magnetic field, or by decreasing the frequency of magnetic field rotation.

This numerical analysis of eq 7 allows one to design the MRS experiments with different materials and estimate the critical parameters such as the critical number of turns or τ-parameter specific for different liquid–nanorod pairs.

3. MATERIALS AND METHODS

HEMA monomer (Sigma-Aldrich Co. LLC) was mixed with the cross-linking agent DEGDMA (Sigma-Aldrich Co. LLC). Five solutions with different concentrations of the cross-linking agent, 1.86, 3, 4.5, 7, and 9.3 wt %, were prepared for testing. The photoinitiator 2,2-dimethoxy-2-phenylacetophenone (Sigma-Aldrich Co. LLC) of 1 wt % relative to the monomers was added to the solutions. Nickel nanorods were synthesized inside pores of alumina membranes (Watman Ltd.) by the electrodeposition technique.[23,31] The synthesis is described in detail in Supporting Information. HEMA solution was added to the beaker with nickel nanorods, and an ultrasound agitation was used to prepare a uniform suspension of nanorods. Concentration of nanorods in the suspension was 0.05 wt %. In order to exclude the interactions between the nanorods, we always double-checked that the chosen nanorod was far away from its neighboors. The distance to the closest nanorod was at least 7 times greater than the nanorod length (see Figure S9 in Supporting Information). This guarantees a weak dependence of nanorod behavior on dipole–dipole interactions as discussed in ref 32. A 1.8 μL droplet of the nanorod dispersion was placed between two glass slides. A 64-μm-thick Kapton tape was inserted between the ends of two glass slides to keep them separated. The drop was sandwiched between glass slides and was investigated under the 50× objective of the BX-51 Olympus microscope. We applied the dark field microscopy technique to detect the 200-nm-diameter nanorods which are not visible in the bright field.[33] First, the microscope was focused on the upper glass slide, and then by moving the objective down, it was focused on the bottom glass slide. This way, it was possible to focus the objective on the magnetic nanorod which was situated in the middle of the optical cell. Each experiment was started by confirming that the tested nanorod was situated at least 20 μm away from each optical slide and the wall effects can be safely neglected. This nanorod position did not change during the HEMA photopolymerization experiment, i.e., the nanorods have never settled down. The following estimates explain these observations. Assuming that the nanorod is settling down at velocity υ and it keeps the long axis parallel to the plates, the drag force on a nanorod is written as $F = 4\pi\eta l\upsilon/\ln(l/d)$.[34] This drag force is balanced by the buoyancy force, $F = \pi d^2 l\Delta\rho g/4$, where $\Delta\rho = 8000$ kg/m^3 is the density difference and g is acceleration due to gravity. Therefore, the settling velocity is estimated as $\upsilon = d^2 l\Delta\rho g \ln(l/d)/(16\eta l) = d^2\Delta\rho g \ln(l/d)/(16\eta)$. Assuming $l/d = 30$, $d = 0.2$ μm, and $\eta = 2$ mPa·s (viscosity prior to photo polymerization), we have $\upsilon = 0.33$ μm/s. If at the first moment a nanorod was positioned in the middle of the optical cell, which is 30 μm away from the bottom plate, it would take about $t \cong 30/0.33 \cong 91$ s to settle down. As shown in the experiments, the HEMA photopolymerization was initiated in less than 10 s after placing the droplet on the glass slide, and it took about 40 s to change the HEMA viscosity 100 times. This explains why the buoyancy effect was insignificant and why we were able to follow the same nanorod during photopolymerization. A supplementary video (Supporting Information S8) shows the behavior of a nanorod subject to the Brownian fluctuations during HEMA photopolymerization in the absence of magnetic field. Mostly in-plane fluctuations were observed, and the nanorod persistently stayed in focus while the film was recorded.

Two magnetic coils orthogonal to each other were used to produce a rotating magnetic field. We used E-66-100 coils (15 mm diameter and 8.5 mm thick, Magnetic Sensor Systems). The current was controlled with a *LabView* program. The design of the setup is described in ref 23. The magnetic field at the center of the optical cell was estimated to be $B = 1.5 \times 10^{-3}$ T. A SPOT videocamera (SPOT Imaging Solutions, Inc.) was used for filming the rotating nanorod during HEMA polymerizaion. In order to initiate the polymerization, the B-100SP UV lamp (UVP, LLC) was placed 100 mm apart from the glass slides containing the HEMA solution. The light intensity at this distance was approximately 10 mW/cm^2. The captured videos were analyzed using *VirtualDub* software (http://www.virtualdub.org).

dx.doi.org/10.1021/la3019474 | *Langmuir* XXXX, XXX, XXX–XXX

Magnetic properties of nickel nanorods vary significantly depending on the parameters of electrodeposition process.[35,36] In order to calculate the magnetic moments of the nickel nanorods, we conducted the MRS experiments in ethylene glycol, a simple Newtonian fluid with η = 16 mPa·s, and used eq 4 to calculate m (for details, see Supporting Information). The obtained magnetic moment appeared to be approximated well by the formula $m = VB\chi/\mu_0$ where V is the nanorod volume, μ_0 is the magnetic permeability of vacuum, and χ is a constant, χ = 92. We also calibrated the MRS viscosity measurements on fluids with known viscosities. First, we measured the bulk viscosity of glycerin (η = 778 mPa·s) and its water mixtures using DV-III Ultra Rheometer (Brookfield Eng.) and then compared the data with the MRS measurements. The results are in a good agreement (see S3 in Supporting Information). These experiments confirmed that we can measure viscosities up to 780 mPa·s with our setup.

After calibration of our MRS system, we obtained the characteristic viscosity η_0 by rotating the nanorod in HEMA solution prior to exposing it to the UV radiation. Once the critical frequency was reached, we solved eq 4 for the viscosity to obtain η_0 = 2.7 mPa·s. This characteristic viscosity did not change when we added the cross-linker.

In all MRS experiments, we were trying to measure the phase lag between the applied signal and nanorod displacement. Our system was unable to detect any phase lag until the nanorod reached N_{cr} revolutions. Therefore, within this time interval the material reacted as a purely viscous liquid, and no fingerprints of material elasticity were observed. With this confirmation in hand, we applied our model to interpret the experimental data.

4. RESULTS

With the obtained parameters, we used the following strategy to evaluate the dependence of characteristic time τ on the cross-linker concentration during UV-polymerization. For each of five solutions, corresponding to 1.86, 3, 4.5, 7, and 9.3 wt % cross-linker concentrations, we obtained the critical number of nanorod revolutions $N_{cr.exp}$. Ten different nanorods with the lengths ranging from 3.9 to 11.85 μm were used in these experiments for each droplet. The diameter of all nanorods was controlled by the diameter of pores in alumina membrane and it was equal to 200.57 ± 2.59 nm (Figure S2(c) in Supporting Information). Then, we ran the numerical analysis of our model, eqs 6, to fit the experimental data using τ as an adjustable parameter of the model. The obtained τ-values were used to plot ten exponential curves for each cross-linker concentration.

In Figure 6a, we plot relative viscosity $\eta(t)/\eta_0$ of HEMA with 1.86 wt % concentration of the cross-linker measured with the MRS and compared these measurements with available data reported in ref 7 for the different powers of UV irradiation. It can be seen that the MRS results are well-fitted by the exponential curve and the relative viscosity curve for our UV source (W = 10 mW/cm^2) is situated between those obtained in ref 7 at stronger UV irradiation with W = 40 mW/cm^2 power and weaker UV irradiation with W = 0.25 mW/cm^2 power. Therefore, the obtained results appear reasonable and coherent with the available data.

In Figure 6b, we plot five dependencies of the relative viscosity, each being related to the given cross-linker content. Any point on these curves represents the average value taken over ten measurements for each concentration of the cross-linker. Error bars provide the standard deviation from the mean value. In the inset, we show the τ-dependence on the cross-linker concentration.

It can be seen from the graphs that the fastest change of viscosity is observed in the system with the highest concentration of the cross-linker. The dependence of the

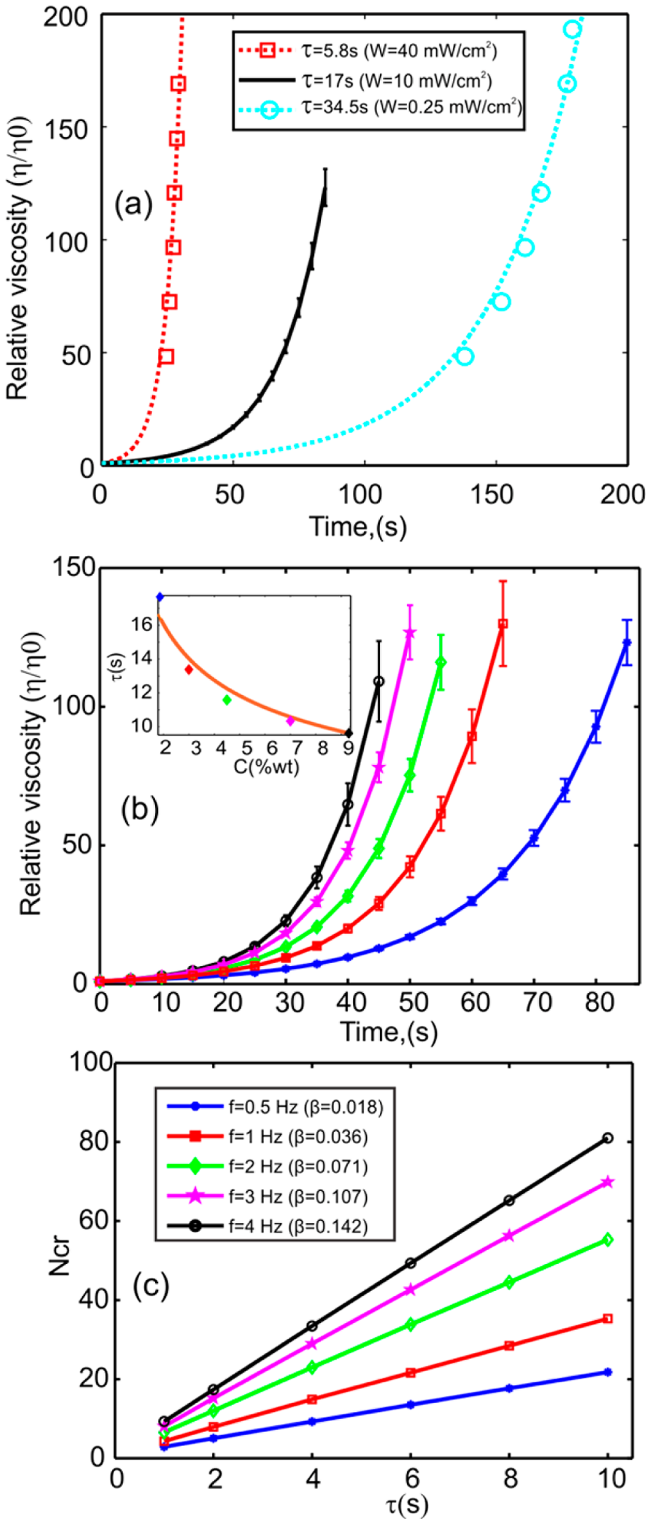

Figure 6. (a) Viscosity change during UV polymerization of HEMA with 1.86 wt % concentration of the cross-linker measured with MRS (f = 0.5 Hz, τ = 17 s) compared with bulk measurements of ref 7 corresponding to τ = 5.8 s and τ = 34.5 s. (b) Viscosity change during UV polymerization for different concentrations of the cross-linker (from the right to the left 1.86, 3, 4.5, 7, 9.3 wt %). Inset: the dependence of characteristic time τ on the weight fraction of the cross-linker, C, in the monomer/cross-linker mixture (diamonds are the experimental points); line is a cubic polynomial fit. (c) Theoretical dependence of the critical number of turns N_{cr} of a nanorod as a function of characteristic time τ.

dx.doi.org/10.1021/la3019474 | Langmuir XXXX, XXX, XXX−XXX

characteristic time τ on the concentration of the cross-linker can be fit with a cubic polynomial $\tau = a \cdot C^{-1/3}$, where $C = m_{cr}/m_{mix}$ is the weight fraction of the cross-linker of weight m_{cr} in the monomer/cross-linker mixture of weight m_{mix} and a = 4.36 s is a coefficient determined from the fit. A theoretical dependence of N_{cr} on τ is shown in the Figure 6c.

This analysis demonstrates that the magnetic rotational spectroscopy allows one to measure the viscosity of polymerized solution when its viscosity drastically changes over a short time interval. However, from the MRS data, one cannot resolve whether the polymer has already undergone the transition to a gel form or it is still a liquid and not completely cross-linked yet. We therefore conducted a series of additional experiments enabling one to distinguish the conformational changes of HEMA solutions at different moments in time.

5. DISCUSSION

HEMA polymerizes through the carbon−carbon double bond and cross-links through the two double bonds in DEGDMA (see Figure S1 in Supporting Information). Therefore, in order to evaluate the cross-linking kinetics, we used FTIR spectroscopy (Nicolet Magna 550). We followed the rate of decrease of carbon−carbon double bonds in the system by measuring the rate of disappearance of the 1635 cm^{-1} peak corresponding to the carbon−carbon double bonds.[37] The intensities of the absorbance peaks were measured before polymerization (solid line in the inset of Figure 7) and after 30, 50, and 60 s of the UV exposure. The dashed line in the inset of Figure 7 shows the intensity of the 1635 cm^{-1} peak after 60 s of photopolymerization.

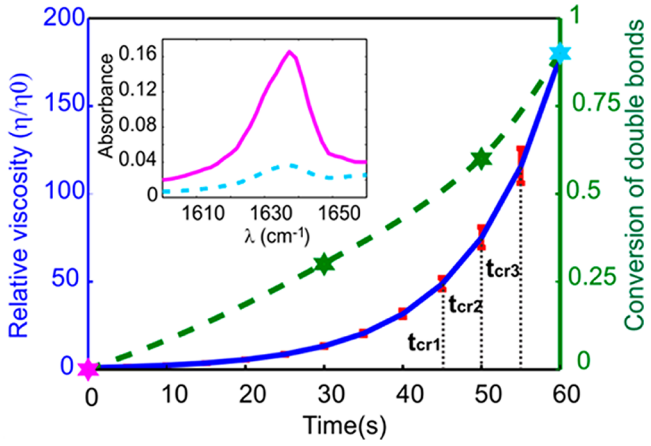

Figure 7. Solid line illustrates the change of relative viscosity with time of photopolymerization of the 4.5 wt % cross-linker solution (left *y*-axis), the stars show the conversion of double bonds during photopolymerization (right *y*-axis), and the dashed line is a trend line. The inset shows a FTIR spectrum of the solution near 1635 cm^{-1} before (solid line) and after 60 s of polymerization (dashed line).

The 1720 cm^{-1} peak corresponding to carbonyl group in HEMA and DEGDMA was used as a reference to calculate the conversion of carbon−carbon bonds in the system, because it does not change during the photopolymerization. Details on the calculations from the FTIR measurements can be found in Supporting Information (see Figure S4). We followed the double bond conversion, ϕ, corresponding to the ratio of the reacted double bonds to the total number of double bonds in the system. The conversion was found from the following equation[37] $\phi = 100 \times (1 - X_t S_0 / X_0 S_t)$, where X_0 and X_t are the areas under the 1638 cm^{-1} peak at time 0 and time t, respectively(integration interval is 1604−1656 cm^{-1}), and S_0 and S_t are the areas under the reference 1720 cm^{-1} peak at time 0 and time t, respectively (integration interval is 1652−1774 cm^{-1}). The conversion of the double bonds ϕ with time is plotted in Figure 7 as the dashed line. We found that the number of double bonds in the solution has decreased by 91.4% after 60 s of photopolymerization. This reduction of the total number of the double bonds in the system is caused by both the linear polymerization of HEMA and cross-linking of HEMA through the double bonds of DEGDMA. However, the FTIR analysis (showing only the total extent of the polymerization) does not provide information on the amount of the polymeric material involved in the cross-linked gel. Therefore, we determined the amount of gel fraction in the polymerizing system as a function of time (Table 1). This fractionation was achieved by washing out the cross-linker, photoinitiator, and a linear polymer from the sample immediately after the photopolymerization. The experimental protocol is described in Supporting Information.

Table 1. Gel Fraction at Different Stages of the Photopolymerization

time of the UV exposure, s	fraction of cross-linked polymer at time t, wt %
45 (t_{cr1} in Figure 7)	23.1 ± 2.11
50 (t_{cr2} in Figure 7)	30.9 ± 2.8
55 (t_{cr3} in Figure 7)	35.7 ± 1.4

Three points in Figure 7, taken at t_{cr1}, t_{cr2}, and t_{cr3} correspond to the time moments when nanorods of different lengths sway back for the first time. As follows from the analysis of Figure 6c, the longer nanorods having greater parameter β stop rotating earlier than the shorter ones. Accordingly, the 6.5 μm long nanorods stopped at time t_{cr1}, the 5.8 μm long nanorods stopped at time t_{cr2}, and then the 3.9 μm long nanorods stopped at time t_{cr3}. The data presented in Table 1 suggest that the longer nanorods most likely probe HEMA having weakly cross-linked gel nuclei, while the shorter nanorods are able to probe HEMA having stronger cross-linked gel domains with the total amount of gel in the suspension reaching ∼36 wt %. Thus, the MRS provides instructive information about the viscosity of polymers undergoing gel formation.

6. CONCLUSIONS

We theoretically developed and implemented a new MRS method which can be used for the in situ (or in vivo) rheological measurements of biofluids and polymer systems when the fluid viscosity increases with time exponentially fast. Only a small quantity of the sample is needed: for example, assuming that the rotating 5-μm-long nanorod can cover the 1 pL volume, one can measure the rheological property of a drop of comparable size. The material rheology can be probed on micro- as well as on nanolevels, depending on the size of the nanorods used. Remarkably, an exponential increase of viscosity can be traced beyond the point when the polymer system undergoes the transition to a gel and the domains start to appear. We showed that the MRS with nanorods probes the viscosity of HEMA when the conversion of double bonds reaches ∼90%. We expect that this method will open new horizons in the quantitative rheological analysis of fluids inside

dx.doi.org/10.1021/la3019474 | Langmuir XXXX, XXX, XXX−XXX

the living cells, microorganisms, and aerosol droplets with thickeners.

■ ASSOCIATED CONTENT

Supporting Information

Additional experiemental information and three videos. This material is available free of charge via the Internet at http://pubs.acs.org.

■ AUTHOR INFORMATION

Corresponding Author

*E-mail address: kkornev@clemson.edu (K. G. Kornev).

Notes

The authors declare no competing financial interest.

■ ACKNOWLEDGMENTS

We thank Guzelia Korneva for suggesting HEMA as a model of rapidly cross-linking polymers, and Daria Monaenkova, Kim Ivey, and David White for their help at different stages of this project. The authors are grateful for the financial support of National Science Foundation (Grants EFRI 0937985 and CMMI-0825773) and the U.S. Air Force contract FA8650-09-D-5900.

■ REFERENCES

(1) Larson, R. G. *The structure and rheology of complex fluids*; Oxford University Press: New York, 1999.

(2) Barabino, G. A.; Platt, M. O.; Kaul, D. K. *Sickle Cell Biomechanics*; Annual Reviews: Palo Alto, 2010; pp 345−367.

(3) Aprelev, A.; Liu, Z. H.; Ferrone, F. A. The Growth of Sickle Hemoglobin Polymers. *Biophys. J.* **2011**, *101* (4), 885−891.

(4) Zavyalova, E. G.; Protopopova, A. D.; Kopylov, A. M.; Yaminsky, I. V. Investigation of Early Stages of Fibrin Association. *Langmuir* **2011**, *27* (8), 4922−4927.

(5) Hall, C. E.; Slayter, H. S. The fibrinogen molecule: its size, shape, and mode of polymerization. *J. Biophys. Biochem. Cytol.* **1959**, *5* (1), 11−16.

(6) Ferri, F.; Greco, M.; Arcovito, G.; Bassi, F. A.; De Spirito, M.; Paganini, E.; Rocco, M. Growth kinetics and structure of fibrin gels. *Phys. Rev. E* **2001**, *63*, 3.

(7) Li, L.; Lee, L. J. Photopolymerization of HEMA/DEGDMA hydrogels in solution. *Polymer* **2005**, *46* (25), 11540−11547.

(8) He, H.; Li, L.; Lee, L. J. Photopolymerization and structure formation of methacrylic acid based hydrogels: The effect of light intensity. *React. Funct. Polym.* **2008**, *68* (1), 103−113.

(9) *Rheology concepts, methods, and applications*; ChemTec Pub.: Toronto, 2006.

(10) Korolev, G. V.; Mogilevich, M. M. *Three-dimensional free-radical polymerization: cross-linked and hyper-branched polymers*; Springer: Berlin, 2009.

(11) Sa, V.; Kornev, K. G. A method for wet spinning of alginate fibers with a high concentration of single-walled carbon nanotubes. *Carbon* **2011**, *49* (6), 1859−1868.

(12) Tsai, C.-C.; Mikes, P.; Andrukh, T.; White, E.; Monaenkova, D.; Burtovyy, O.; Burtovyy, R.; Rubin, B.; Lukas, D.; Luzinov, I.; Owens, J. R.; Kornev, K. G. Nanoporous Artificial Proboscis for Probing Minute Amount of Liquids. *Nanoscale* **2011**, *3* (11), 4685−4695.

(13) Wilhelm, C.; Gazeau, F.; Bacri, J. C. Rotational magnetic endosome microrheology: Viscoelastic architecture inside living cells. *Phys. Rev. E* **2003**, *67*, 6.

(14) Bausch, A. R.; Möller, W.; Sackmann, E. Measurement of Local Viscoelasticity and Forces in Living Cells by Magnetic Tweezers. *Biophys. J.* **1999**, *76* (1), 573−579.

(15) Guigas, G.; Kalla, C.; Weiss, M. Probing the Nanoscale Viscoelasticity of Intracellular Fluids in Living Cells. *Biophys. J.* **2007**, *93* (1), 316−323.

(16) Weihs, D.; Mason, T. G.; Teitell, M. A. Bio-Microrheology: A Frontier in Microrheology. *Biophys. J.* **2006**, *91* (11), 4296−4305.

(17) Barrera, C.; Florian-Algarin, V.; Acevedo, A.; Rinaldi, C. Monitoring gelation using magnetic nanoparticles. *Soft Matter* **2010**, *6* (15), 3662−3668.

(18) Erglis, K.; Ose, V.; Zeltins, A.; Cebers, A. Viscoelasticity of the bacteriophage Pf1 network measured by magnetic microrheology. *Magnetohydrodynamics* **2010**, *46* (1), 23−29.

(19) Huisman, E. M.; Wen, Q.; Wang, Y.-H.; Cruz, K.; Kitenbergs, G.; Erglis, K.; Zeltins, A.; Cebers, A.; Janmey, P. A. Gelation of semiflexible polyelectrolytes by multivalent counterions. *Soft Matter* **2011**, *7* (16), 7257−7261.

(20) McNaughton, B. H.; Agayan, R. R.; Wang, J. X.; Kopelman, R. Physiochemical microparticle sensors based on nonlinear magnetic oscillations. *Sens. Actuators, B: Chem.* **2007**, *121* (1), 330−340.

(21) Samouhos, S.; McKinley, G. Carbon nanotube-magnetite composites, with applications to developing unique magnetorheological fluids. *J. Fluid Eng.: Trans. ASME* **2007**, *129* (4), 429−437.

(22) Korneva, G.; Ye, H. H.; Gogotsi, Y.; Halverson, D.; Friedman, G.; Bradley, J. C.; Kornev, K. G. Carbon nanotubes loaded with magnetic particles. *Nano Lett.* **2005**, *5* (5), 879−884.

(23) Tokarev, A.; Rubin, B.; Bedford, M.; Kornev, K. G. Magnetic Nanorods for Optofluidic Applications; *AIP Conference Proceedings*, 2010; Vol *1311*, pp 204−209.

(24) Allione, M.; Torre, B.; Casu, A.; Falqui, A.; Piacenza, P.; Di Corato, R.; Pellegrino, T.; Diaspro, A. Rod-shaped nanostructures based on superparamagnetic nanocrystals as viscosity sensors in liquid. *J. Appl. Phys.* **2011**, *110* (6).

(25) Frka-Petesic, B.; Erglis, K.; Berret, J. F.; Cebers, A.; Dupuis, V.; Fresnais, J.; Sandre, O.; Perzynski, R. Dynamics of paramagnetic nanostructured rods under rotating field. *J. Magn. Magn. Mater.* **2011**, *323* (10), 1309−1313.

(26) Anguelouch, A.; Leheny, R. L.; Reich, D. H. Application of ferromagnetic nanowires to interfacial microrheology. *Appl. Phys. Lett.* **2006**, *89* (11), 111914.

(27) Landau, L. D.; Lifshitz, E. M. *Electrodynamics of continuous media*; Pergamon: Oxford, 1960.

(28) Blums, E.; Cebers, A.; Maiorov, M. M. *Magnetic fluids*; Walter de Gruyter: New York, 1997.

(29) Doi, M.; Edwards, S. F. *The theory of polymer dynamics*; Clarendon Press: Oxford, 1988.

(30) Paivo, K.; Irene, S.; Brandon, H. M.; Raoul, K. High frequency asynchronous magnetic bead rotation for improved biosensors. *Appl. Phys. Lett.* **2010**, *97* (22), 223701.

(31) Bentley, A. K.; Ellis, A. B.; Lisensky, G. C.; Crone, W. C. Suspensions of nickel nanowires as magneto-optical switches. *Nanotechnology* **2005**, *10*, 2193.

(32) Kornev, K. G.; Halverson, D.; Korneva, G.; Gogotsi, Y.; Fridman, G. Magnetostatic interactions between carbon nanotubes filled with magnetic nanoparticles. *Appl. Phys. Lett.* **2008**, *92*, 233117.

(33) Innoue, S. *Video Microscopy: The Fundamentals (Language of Science)*, 2nd ed.; Springer: New York, 1997.

(34) Doi, M.; Edwards, S. F. *The theory of polymer dynamics*; Oxford University Press: London, 1986.

(35) Prina-Mello, A.; Diao, Z.; Coey, J. Internalization of ferromagnetic nanowires by different living cells. *J. Nanobiotechnol.* **2006**, *4* (1), 1−11.

(36) Hultgren, A.; Tanase, M.; Felton, E. J.; Bhadriraju, K.; Salem, A. K.; Chen, C. S.; Reich, D. H. Optimization of yield in magnetic cell separations using nickel nanowires of different lengths. *Biotechnol. Prog.* **2005**, *21* (2), 509−515.

(37) Ghaemy, M.; Heidaripour, M.; Barghamadi, M. Synthesis, characterization, and cure reaction of methacrylate-based multifunctional monomers for dental composites. *J. Appl. Polym. Sci.* **2007**, *106* (3), 1917−1923.